



Universiteit
Leiden
The Netherlands

Targeting the adenosinergic system: Ligand binding kinetics and label-free assays for the study of SLC29A1 transporter and A2B adenosine receptor

Vlachodimou A.

Citation

Targeting the adenosinergic system: Ligand binding kinetics and label-free assays for the study of SLC29A1 transporter and A2B adenosine receptor. (2020, November 4). *Targeting the adenosinergic system: Ligand binding kinetics and label-free assays for the study of SLC29A1 transporter and A2B adenosine receptor.* Retrieved from <https://hdl.handle.net/1887/138132>

Version: Publisher's Version

License: [Licence agreement concerning inclusion of doctoral thesis in the Institutional Repository of the University of Leiden](#)

Downloaded from: <https://hdl.handle.net/1887/138132>

Note: To cite this publication please use the final published version (if applicable).

Cover Page



Universiteit Leiden



The handle <http://hdl.handle.net/1887/138132> holds various files of this Leiden University dissertation.

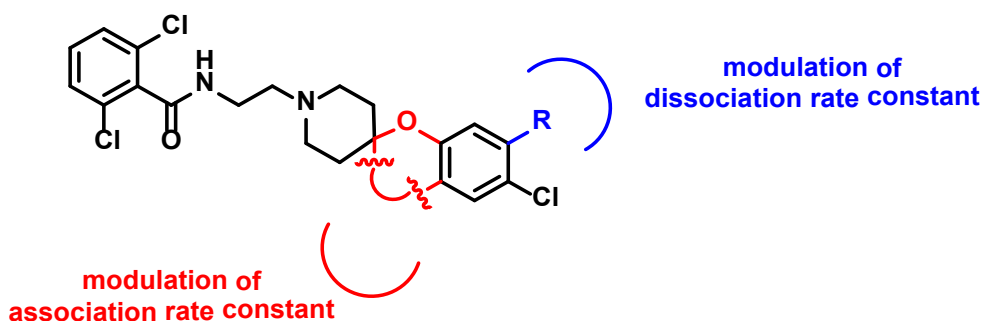
Author: Vlachodimou, A.

Title: Targeting the adenosinergic system: Ligand binding kinetics and label-free assays for the study of SLC29A1 transporter and A2B adenosine receptor

Issue Date: 2020-11-04

Chapter 6

Kinetic profiling of novel spirobenzo-oxazinepiperidinone derivatives as Equilibrative Nucleoside Transporter 1 inhibitors



*Anna Vlachodimou, Jara Bouma, Michel De Cleyn,
Didier Berthelot, Stefan Pype, Jean-Paul Bosmans,
Herman van Vlijmen, Berthold Wroblowski,
Laura H. Heitman, and Adriaan P. IJzerman*

Manuscript in preparation

Abstract

Evaluation of binding kinetics parameters, k_{on} , k_{off} and residence time (RT), in addition to the traditional *in vitro* parameter of affinity is receiving increased attention in the early stages of drug discovery. It emerges as a meaningful measure for the evaluation of a ligand's duration of action and more generally drug efficacy and safety. We report the biological evaluation of a novel series of spirobenzo-oxazinepiperidinone derivatives as inhibitors of the equilibrative nucleoside transporter 1 (ENT1). The compounds were evaluated in radioligand binding experiments, *i.e.* displacement, competition association and wash-out assays, to evaluate their affinity and binding kinetics parameters. In this way a complete structure-kinetics relationship (SKR) study was performed alongside a more classical SAR analysis with respect to ENT1 binding. Among the 29 compounds tested, **28** stood out with high affinity and a residence time of 87 min. These findings reveal the importance of supplementing affinity data with binding kinetics at transport proteins such as ENT1.

Introduction

Nucleosides are critical endogenous molecules that are formed by fusion of pyrimidines or purine bases with either a ribose or deoxyribose sugar moiety. Subsequent phosphorylation converts the molecules into nucleotides. Both nucleosides and nucleotides serve as metabolic precursors in the synthesis of nucleic acids, play a crucial role in energy metabolism, or are involved in signaling pathways and enzyme regulation and metabolism^{1, 2}. Due to the important physiological role of nucleosides, nucleoside analogues have been introduced as therapeutic molecules. They have been and are a core strategy in the treatment of cancer and viral infections³. By mimicking the uptake of nucleosides, they incorporate into the newly synthesized DNA which results in chain termination and apoptosis⁴⁻⁶.

The translocation of nucleosides and nucleoside analogues inside and outside of cell membranes occurs via two nucleoside transporter (NT) families; the concentrative (CNTs; SLC28) and the equilibrative NTs (ENTs; SLC29). In addition, NTs are involved in the recycling of nucleosides in cells lacking *de novo* synthesis, such as erythrocytes⁷. Human (h) ENT1 (SLC29A1) is the best-studied ENT and the major plasma membrane nucleoside transporter, highly expressed in tissues such as erythrocytes, vascular endothelium and the gastrointestinal tract^{2, 8, 9}. It translocates its substrates over the plasma membrane in a bidirectional, sodium-independent manner by following the concentration gradient in order to establish equilibrium^{10, 11}.

Pharmacological inhibition of hENT1 could be a promising therapeutic strategy for many diseases. Due to its increased expression in a variety of cancers, e.g. breast cancer¹² and pancreatic adenocarcinoma¹³, the use of ENT1 inhibitors presents a potential anti-cancer therapy¹⁴. As an alternative and add-on cancer therapy the administration of hENT1 inhibitors in combination with anti-cancer nucleoside drugs transported by other NTs has been proposed. Such combination therapy would enhance the effect of nucleoside drugs by preventing cellular efflux, as well as reduce the occurrence of drug resistance^{4, 10}. Lastly, ENT1 inhibition has therapeutic benefits by the modulation of the extracellular concentration of adenosine⁸. Clinical trials with draflazine, an ENT1 inhibitor, showed promising results in patients with unstable coronary disease, by enhancing the anti-ischemic and cardioprotective effects of endogenous adenosine¹⁵. Two potent ENT1 inhibitors, dilazep and dipyridamole, are already on the market as vasodilators^{16, 17}, but the development of novel inhibitors with improved efficacy and selectivity is desired².

It is increasingly realized that ligand selection based solely on affinity, an equilibrium parameter, is not necessarily a good predictor for *in vivo* efficacy. Contrarily, the study of ligand binding kinetics, *i.e.* association, k_{on} , and dissociation, k_{off} , rate constants as well as residence time (RT), on a majority of targets, including enzymes and G protein-coupled receptors (GPCRs), has provided emerging evidence that *in vivo* efficacy is often linked to optimized binding kinetics parameters of the ligand¹⁸⁻²⁰. Although the binding kinetics of some ENT1 inhibitors have been studied², their incorporation in drug discovery efforts, *i.e.* by constructing structure-kinetics (SKR)

next to the structure-affinity relationships (SAR), has been limited²¹.

In this study, we report the biological evaluation of a novel series of spirobenzo-oxazinepiperidinone derivatives, as hENT1 inhibitors with a structure different to the marketed products dilazep and dipyridamole. These compounds were evaluated in a radioligand displacement assay to determine their affinity and in a radioligand competition association and wash-out assay that enabled their kinetic characterization. We learned that both the speed of target engagement and the dissociation of the ligand-transporter complex play a distinctive role in the compounds' affinities.

Results and Discussion

Radioligand binding assays to determine affinity and target binding kinetics

The binding affinity of all compounds was determined on human erythrocyte membranes in the presence of 4 nM of the tritium-labeled ENT1 inhibitor 4-nitrobenzylthioinosine (NBTI). All compounds were found to inhibit specific radioligand binding to the hENT1 transporter and the determined affinities are listed in Tables 1 till 3. The compounds had moderate to high affinity for the transporter ranging from 1039 nM for compound **20** to 0.58 nM for compound **29**.

Subsequently, all compounds with affinity values lower than 100 nM were evaluated in a radioligand competition association assay, to determine the kinetic parameters k_{on} and k_{off} . This assay is based on the Motulsky and Mahan model and characterizes the time-dependent binding of two competing ligands on the same target binding site²². For the purposes of the assay, the specific binding of [³H]NBTI was measured at different time points during an incubation of 60 minutes in the absence and presence of an IC₅₀ concentration of the competing inhibitor. Figures 1A and 1B present the curves from inhibitors **18**, **23** and **25** with similar, shorter and longer RTs compared to the radioligand used [³H]NBTI, respectively. A long RT compound presents a characteristic overshoot followed by a steady decrease in specific radioligand binding, which eventually reaches equilibrium around 50%. A medium RT compound, between 20 and 30 minutes in this case, displays a curve with a similar shape to the control curve of [³H]NBTI (RT~27 min), while a shallow, slowly ascending curve is typical for compounds with a short RT.

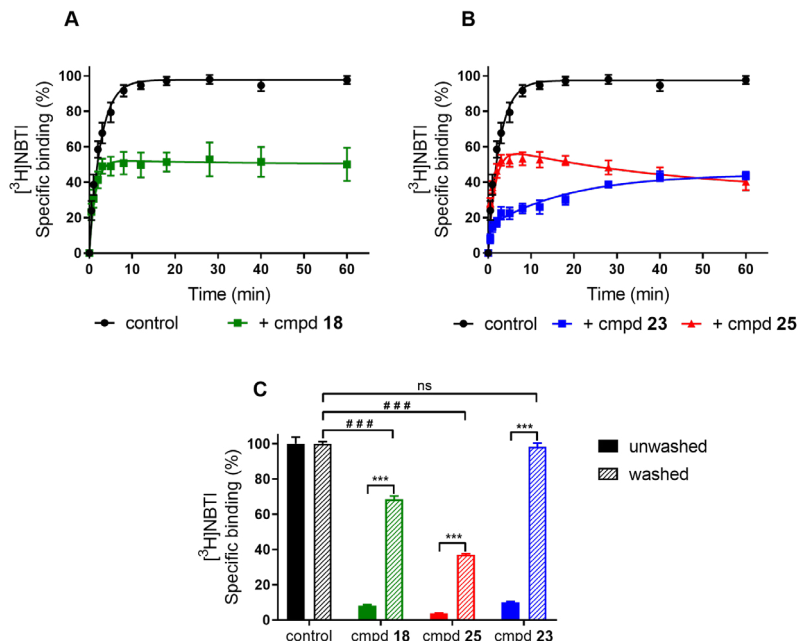


Figure 1: Competition association of specific [^3H]NBTI binding to ENT1 transporter on erythrocyte membranes (10°C) in the absence or presence of IC_{50} concentration of a similar (A), shorter and longer (B) RT compound (cmpd) compared to the control. Ligand binding of compounds at $10\times\text{IC}_{50}$ concentration before and after washing step, compared to the control radioligand binding without the presence of any competitor (C). Data are shown as mean \pm SEM from at least three independent experiments performed in duplicate. *** $p \leq 0.0001$ determined in an unpaired t-test with Welch's correction. ### $p \leq 0.0001$ determined in an one-way ANOVA test with Dunnett's correction.

Structure-Affinity Relationships (SAR) and Structure-Kinetic Relationships (SKR).

Substitution on the 4-position of the phenyl ring (compounds 1 - 25).

The obtained affinities (K_i values) and kinetic profiles (k_{on} , k_{off} values and RTs) were used to derive SAR and SKR of the ENT1 inhibitors. In this series of compounds, phenyl ring analysis consisted of an extensive substitution on the 4-position by different side chains, represented by R groups (Table 1-2). Substitution of a primary amine (**1**) to the phenyl ring resulted in a modest affinity of 145 nM and therefore the RT was not determined. Introduction of a secondary or tertiary amine by substitution of one (**2**) or two (**3**) methyl groups resulted in an approximately 30-fold increase in affinity, and a short RT for both compounds. Addition of an acetamide to the phenyl ring (**4**) led to a reduced affinity compared to **2** and **3**, while RT remained short. Association rate constant k_{on} was decreased by 10- and 13-fold vs **2** and **3**, respectively. Addition of a methoxymethyl (**5**) increased both the affinity and

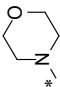
RT compared to **4**, to values similar to the ones of secondary and tertiary amine substitution. The greatest increase in both affinity and RT was obtained when substituting a cyclopentyl group, either directly (**6**) or with an additional carbon (**7**) to the secondary amine. Changes in k_{on} were also observed, with **7** presenting a 2-fold decrease compared to **6**.

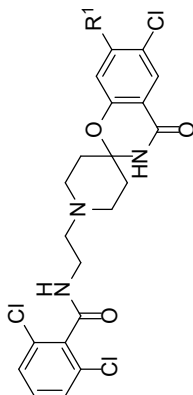
As the longer bulkier side chains of **6** and **7** resulted in an increased RT, a longer amine substituent was introduced. A propyl-amine spacer was added to the aromatic amine and its substitution yielded compounds **8** to **10** (Table 1). Compound **8** consisted of a secondary amine with a methyl group as substituent and its affinity was 30 nM, while the RT was short (3.4 min). Further substitution of the propyl-amine spacer (**9**, **10**) led to an increased affinity and RT compared to inhibitor **8**. Specifically, the addition of a *tert*-butyloxycarbonyl (BOC) group and a methyl to the amine (**10**), led to an affinity of less than 2 nM and a RT of 26 minutes, comparable to inhibitors **6** and **7**. All in all, the increased substituent size of compounds **8** to **10**, led to an increased affinity, in addition to an increased association and decreased dissociation rate constant.

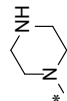
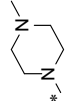
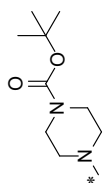
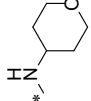
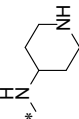
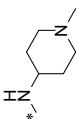
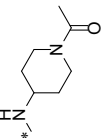
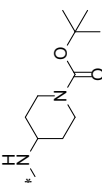
A combination of the cyclic characteristics of compounds **6** and **7** with the three carbon amine linker of compounds **8** to **10** that exhibited an increase in affinity and RT, led to the design and synthesis of inhibitors **11** to **19** (Table 1). The morpholino group of compound **11** and the *para*-substituted piperazines of **12** to **14**, resulted in similar k_{on} values, whereas k_{off} values and as a consequence RT differed up to 13-fold, with the BOC-group (**14**) yielding the longest RT of all four compounds. For compounds **15** to **19**, the aromatic amine was substituted with tetrahydropyran (**15**) or a substituted piperidine (**16** to **19**) and therefore, the functional groups are located four positions away from the amide, comparable to the inhibitors with a three-carbon linker. Similar as for inhibitors **12** and **13**, the compounds with a secondary (**16**) or tertiary (**17**) amine in the ring showed a relatively modest affinity and a fast dissociation from the target. The N-acetyl (**18**) and the N-BOC-group (**19**) both caused a high affinity and a long RT, comparable to **14**.

In addition to the results obtained with the subseries of the amine-substituted phenyl ring, an oxygen linker was introduced, leading to inhibitors **20** to **25** (Table 2). Introducing a hydroxyl group (**20**) resulted in a significantly decreased affinity (K_i = 1039 nM) and therefore the binding kinetics were not measured. Substitution of the phenyl's 4-position with an ether with bigger nonpolar groups (**21**, **22**) increased the affinity to the nanomolar range. The binding kinetics for isopropyl-substituted **21** were fast for both the association and dissociation to and from the target. In contrast cyclopentyl-substituted **22** presented a slower association and dissociation rate constant. In addition, an oxygen linker was used to connect the main scaffold with *para* substituted piperidines. The piperidine (**23**) and N-methylpiperidine (**24**) derivatives showed a similar association rate constant and a fast dissociation of less than 5 minutes. The N-acetylpiperidine (**25**) analogue yielded both a slow association and dissociation rate, resulting in a RT of 72 minutes, the longest in this series.

Table 1: Affinity (pK_i) and Kinetic Parameters (k_{on} , k_{off} , RT) of ENT1 inhibitors **1** – **19**.

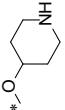
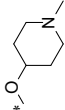
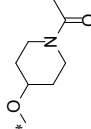
| compd | R ¹ | pK_i^a (Ki (nM)) | k_{on} (nM ⁻¹ min ⁻¹) ^a | k_{off} (min ⁻¹) ^a | RT (min) ^{a,b} | K_D (nM) ^{a,c} |
|-----------|--------------------------------------------------------------------------------------|--------------------|-------------------------------------------------------------|---------------------------------------------|-------------------------|---------------------------|
| 1 | NH ₂ | 6.84 ± 0.04 (145) | N.D. ^d | N.D. | N.D. | N.D. |
| 2 | NHCH ₃ | 8.29 ± 0.02 (5.1) | 0.123 ± 0.029 | 0.203 ± 0.047 | 4.9 ± 1.1 | 1.65 ± 0.55 |
| 3 | N(CH ₃) ₂ | 8.51 ± 0.02 (3.1) | 0.158 ± 0.048 | 0.151 ± 0.020 | 6.6 ± 0.9 | 0.95 ± 0.31 |
| 4 | NHCOCH ₃ | 7.18 ± 0.02 (67) | 0.012 ± 0.006 | 0.386 ± 0.107 | 2.6 ± 0.7 | 33.2 ± 18.9 |
| 5 | NHCH ₂ OCH ₃ | 8.13 ± 0.05 (7.4) | 0.036 ± 0.006 | 0.185 ± 0.023 | 5.4 ± 0.7 | 5.10 ± 1.08 |
| 6 | NH(cPentyl) | 8.97 ± 0.14 (1.1) | 0.101 ± 0.035 | 0.048 ± 0.003 | 21 ± 1.4 | 0.48 ± 0.17 |
| 7 | NHCH ₂ (cPentyl) | 8.63 ± 0.09 (2.3) | 0.045 ± 0.008 | 0.037 ± 0.002 | 27 ± 1.2 | 0.84 ± 0.16 |
| 8 | NH(CH ₂) ₃ NHCH ₃ | 7.52 ± 0.04 (30) | 0.011 ± 0.004 | 0.296 ± 0.050 | 3.4 ± 0.6 | 26.0 ± 9.40 |
| 9 | NH(CH ₂) ₃ NHCOCH ₃ | 8.23 ± 0.05 (5.9) | 0.025 ± 0.005 | 0.096 ± 0.008 | 10 ± 0.9 | 3.80 ± 0.79 |
| 10 | NH(CH ₂) ₃ N(CH ₃)COOtBu | 8.77 ± 0.04 (1.7) | 0.033 ± 0.003 | 0.038 ± 0.003 | 26 ± 2.0 | 1.15 ± 0.14 |
| 11 |  | 8.75 ± 0.04 (1.8) | 0.040 ± 0.006 | 0.064 ± 0.014 | 16 ± 3.3 | 1.63 ± 0.41 |



| | | | | | | |
|-----------|--------------------------------------------------------------------------------------|-------------------|---------------|---------------|-----------|-------------|
| 12 |  | 7.92 ± 0.03 (12) | 0.038 ± 0.004 | 0.350 ± 0.026 | 2.9 ± 0.2 | 9.29 ± 1.29 |
| 13 |  | 8.40 ± 0.08 (4.0) | 0.027 ± 0.004 | 0.089 ± 0.004 | 11 ± 0.5 | 3.30 ± 0.52 |
| 14 |  | 8.67 ± 0.04 (2.1) | 0.020 ± 0.001 | 0.027 ± 0.010 | 38 ± 14 | 1.34 ± 0.50 |
| 15 |  | 8.37 ± 0.05 (4.3) | 0.033 ± 0.008 | 0.100 ± 0.007 | 10 ± 0.7 | 3.03 ± 0.81 |
| 16 |  | 7.35 ± 0.07 (44) | 0.016 ± 0.002 | 0.464 ± 0.092 | 2.2 ± 0.4 | 29.6 ± 7.32 |
| 17 |  | 7.35 ± 0.03 (44) | 0.022 ± 0.002 | 0.535 ± 0.031 | 1.9 ± 0.1 | 24.5 ± 2.94 |
| 18 |  | 8.53 ± 0.03 (2.9) | 0.026 ± 0.003 | 0.038 ± 0.009 | 26 ± 6.5 | 1.47 ± 0.41 |
| 19 |  | 8.73 ± 0.06 (1.9) | 0.019 ± 0.001 | 0.030 ± 0.009 | 34 ± 9.7 | 1.52 ± 0.45 |


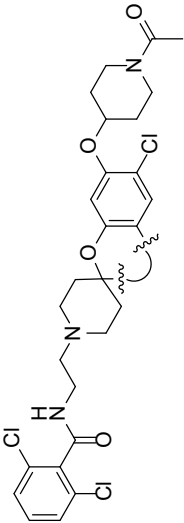
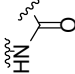
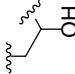


^aValues represent the mean ± SEM of at least three individual experiments, performed in duplicate. ^bRT = 1/ k_{off} . ^cKinetic K_D values, defined as $K_D = k_{off}/k_{on}$. ^dN.D. = not determined.

Table 2: Affinity (pK_i) and Kinetic Parameters (k_{on} , k_{off} , RT) of ENT1 inhibitors **20** – **25**.

| cmpd | R ² | pK_i^a (Ki (nM)) | k_{on} (nM ⁻¹ min ⁻¹) ^a | k_{off} (min ⁻¹) ^a | RT (min) ^{a,b} | K_D (nM) ^{a,c} |
|-----------|-------------------------------------------------------------------------------------|--------------------|-------------------------------------------------------------|---------------------------------------------|-------------------------|---------------------------|
| 20 | OH | 5.98 ± 0.36 (1039) | N.D. ^d | N.D. | N.D. | N.D. |
| 21 | O-CH(CH ₃) ₂ | 8.84 ± 0.11 (1.5) | 0.130 ± 0.051 | 0.056 ± 0.011 | 18 ± 3.6 | 0.43 ± 0.19 |
| 22 | O-c-Pentyl | 8.62 ± 0.09 (2.4) | 0.029 ± 0.007 | 0.029 ± 0.006 | 35 ± 7.6 | 0.99 ± 0.32 |
| 23 |  | 8.22 ± 0.02 (6.1) | 0.122 ± 0.040 | 0.204 ± 0.051 | 4.9 ± 1.2 | 1.66 ± 0.69 |
| 24 |  | 8.06 ± 0.06 (8.7) | 0.127 ± 0.020 | 0.414 ± 0.085 | 2.4 ± 0.5 | 3.26 ± 0.84 |
| 25 |  | 8.65 ± 0.06 (2.2) | 0.032 ± 0.004 | 0.014 ± 0.003 | 72 ± 14 | 0.43 ± 0.10 |

^aValues represent the mean ± SEM of at least three individual experiments, performed in duplicate. ^bRT = $1/k_{off}$ ^cKinetic K_D values, defined as $K_D = k_{off}/k_{on}$. ^dN.D. = not determined

Table 3: Affinity (pK_i) and Kinetic Parameters (k_{on} , k_{off} , RT) of ENT1 inhibitors **25** – **29** with modifications on the main ring.

| compd |  | pK_i^a (KI (nM)) | k_{on} (nM ⁻¹ min ⁻¹) ^a | k_{off} (min ⁻¹) ^a | RT (min) ^{a,b} | K_D (nM) ^{a,c} |
|-----------|--------------------------------------------------------------------------------------|--------------------|-------------------------------------------------------------|---------------------------------------------|---------------------------|---------------------------|
| 25 |  | 8.65 ± 0.06 (2.2) | 0.032 ± 0.004 | 0.014 ± 0.003 | 72 ± 14 | 0.43 ± 0.10 |
| 26 |  | 8.73 ± 0.03 (1.9) | 0.043 ± 0.008 | 0.015 ± 0.005 | 66 ± 20 | 0.35 ± 0.12 |
| 27 |  | 8.99 ± 0.09 (1.0) | 0.054 ± 0.015 | 0.013 ± 0.003 | 79 ± 20 | 0.23 ± 0.09 |
| 28 |  | 9.23 ± 0.03 (0.59) | 0.097 ± 0.007 | 0.011 ± 0.001 | 87 ± 8.7 | 0.12 ± 0.01 |
| 29 |  | 9.24 ± 0.07 (0.58) | 0.095 ± 0.020 | 0.019 ± 0.007 | 52 ± 20 | 0.20 ± 0.09 |

^aValues represent the mean ± SEM of at least three individual experiments, performed in duplicate. ^b $RT = 1/k_{off}$ ^cKinetic K_D values, defined as $K_D = k_{off}/k_{on}$.

Substitution on the main ring (compounds 25 – 29).

After the exploration of the right-hand side of the scaffold, changes on the main ring were introduced in order to evaluate their significance in the SAR and SKR. As the N-acetylpiperidine ether at the 4-position of the phenyl ring (**25**) caused the longest RT as well as a high affinity, it was maintained as the R-substitution, while alterations were performed to the main ring (Table 3). A reduction of polarity of the ring led (**26-29**) to an increased affinity as well as an increase in association rate constant. However, the RTs stayed within the same (long) range as **25**, where compound **28** had the longest RT of 87 minutes.

Washout assay

A washout assay was used to validate the findings in the competition association assays (Figure 1C). Three chemically-related inhibitors differing only at the 4-phenyl substituent, not the main ring, yet with distinct RTs were examined, *i.e.* compound **25** presenting a long RT, compound **18** with a medium RT (similar to the radioligand) as well as compound **23** that displayed a short RT. Following an 1 h pre-incubation with a $10 \times IC_{50}$ concentration of compound and four subsequent wash and centrifugation cycles, [³H]NBTI was co-incubated and radioligand binding was determined. The unwashed condition was also assessed, where no wash and centrifugation cycle occurred before the determination of radioligand binding. The results of both washed and unwashed samples were compared to the control condition without any competitor (100% washed and unwashed radioligand binding, respectively).

All inhibitors showed a significant increase in [³H]NBTI binding after four extensive washing steps, suggesting all inhibitors were washed away to some extent due to dissociation from the target. The recovery of [³H]NBTI binding increased in relation to the inhibitor's duration of binding to the target. Long RT inhibitor **25** was washed away only 37% after four extensive washing steps, suggesting that more than 60% of the inhibitor was still bound to the target. To the contrary, short RT inhibitor **23** was completely washed away, as the radioligand was found to bind to all target after the washing steps. Compound **18** displayed an intermediate behavior with approx. 60% being washed away. These findings are in line with the data from the competition association assay. Additionally, this confirms that the RT is determined by binding to ENT1 and not rebinding, since all unbound inhibitor molecules are taken out of the sample with washing. A possible occurrence of rebinding would also require a correlation between lipophilicity (logD) and association rate constants, since lipophilic compounds are more likely to bind to the plasma membrane²³. By binding to the plasma membrane, drug concentration would locally increase and rise around the target, which facilitates the approach of the inhibitor to the transporter and subsequently prolong the pharmacological effect^{24, 25}. However, no such correlation between lipophilicity and association rate constants was observed (see Supplementary Figure S2), making membrane binding of these compounds less probable.

Kinetic map

In an effort to obtain a better comparison of kinetic and affinity parameters, a kinetic map was created (Figure 2). In this map, the association (x-axis) together with the dissociation (y-axis) and the kinetic affinity (diagonal lines) values were plotted. Based on this representation the compounds can be divided into three sub-groups. Inhibitors that belong to group A display similar association rate constants, but differ in their affinity for ENT1 due to diverse dissociation rate constants. As RT has been proven a predicting tool for *in vivo* efficacy, many SKR studies have been directed towards optimization of dissociation rates in order to create a kinetically favorable ligand²⁶. However, lately more attention has been given to the association rate constant as well, as it also plays a role in drug efficacy, due to possible increased rebinding and / or increased drug-target selectivity^{20, 25, 27}. In addition, k_{on} has been described to be crucial for high receptor occupancy ('target engagement') and thus even a longer duration of action²⁷⁻²⁹.

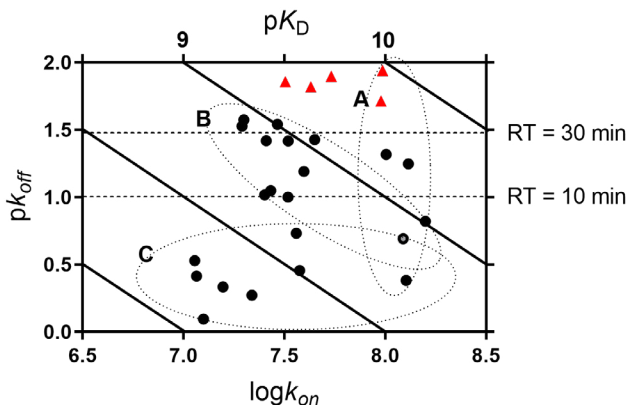


Figure 2: Kinetic map of all ENT1 inhibitors that were kinetically characterized through [³H] NBTI competition association assays. The kinetically derived affinity (K_D) is represented by the diagonal parallel lines. The compounds are dividing into short, medium and long RT by the horizontal dashed lines, indicating a RT of 10 and 30 minutes. Group A: inhibitors that display similar k_{on} values but because of different k_{off} values have divergent K_D values. Group B: inhibitors with similar K_D values despite presenting diverse k_{off} and k_{on} values. Group C: inhibitors showing similar k_{off} values but due to differences in k_{on} have different K_D values. The red triangles correspond to inhibitors with modifications in the main ring.

For that reason, the construction of a kinetic map allows for the identification of compounds that present the preferred dissociation and association rate constants. Inhibitors in group B have similar affinities but have many different combinations in association and dissociation rate constants. For example, inhibitors **3** and **22** have similar kinetic affinities (0.95 and 0.99 nM, respectively), yet their RTs are 5-fold different with corresponding k_{off} values of 0.151 and 0.029 min⁻¹, respectively. In

case of a simple SAR study, these inhibitors would have been considered similar and been treated equally in e.g. the triage of further compound selection. In fact, this is an issue in many drug discovery programs, in which medicinal chemists arrive at series of compounds with high but (seemingly) similar affinity. In addition, a simple SAR study may not necessarily result in “correct” affinities for compounds with extreme binding kinetics, as it has been previously reported²¹.

Therefore, SAR should be complemented with SKR studies at the early stages of drug discovery to allow for a more thorough and complete classification of compounds, from which a more informed follow-up is possible. Lastly, group C represents inhibitors that exhibit fast dissociation rate constants but differ in their affinity for ENT1 due to divergent association rate constants. The blue dots represent the inhibitors with modifications in the main ring. These follow a similar pattern as group A, where the association rate constants cause the difference in affinity. However, they are separated from group A by having a long RT over 30 minutes in contrast to less than 10 minutes for group A.

Correlation plots

To gain further insight into the relationship between the parameters, correlation plots were constructed (Figure 3). The affinity obtained from the typical radioligand displacement assay (pK_i) and the one calculated from the kinetic parameters (pK_D) obtained from the radioligand competition association assay were found to be significantly correlated (Figure 3A), validating the use of the competition association assay. In addition, the association rate constants ($\log k_{on}$) of inhibitors **1 - 25** were plotted against their kinetic affinity (pK_D) (Figure 3B), which showed a low, non-significant correlation ($r=0.38$, $P=0.068$). On the contrary, plotting the dissociation rate constants (pK_{off}) and the kinetic affinity (pK_D) demonstrated a strong correlation ($r=0.83$, $P<0.0001$) (Figure 3C). As far as the modifications in the main ring are concerned, the correlations are opposite to the aforementioned. Association rate constants and affinity were strongly correlated for the inhibitors **25 - 29** ($r=0.92$, $P=0.026$) (Figure 3D), while dissociation rate constants and affinity seem completely uncorrelated (Figure 3E). The two plots together illustrate that the R substituents may be responsible for long lasting binding and hence a longer pharmacological effect of the inhibitors, whereas the composition of the main ring is responsible for a fast binding to the target and an immediate effect. These findings become of importance when the disease to be treated is taken into account.

In the case of an acute disease, such as myocardial infarction, there is a need for a fast associating drug which immediately exerts its effect. On the other hand, for a chronic disease such as cancer a slow dissociation is desired to maintain a longer physiological effect³⁰. If the RT exceeds the pharmacokinetic half-life, the drug can continue to have a sustained pharmacodynamic effect after plasma clearance. This, in principle, provides advantages like convenient dosing schedules for patients as

well as preventing off-target toxicities^{20, 31}. However, association rates should not be neglected even in the case of a chronic disease. The competition between the drug and the often high concentrations of the endogenous ligand may require a fast association rate of the drug.

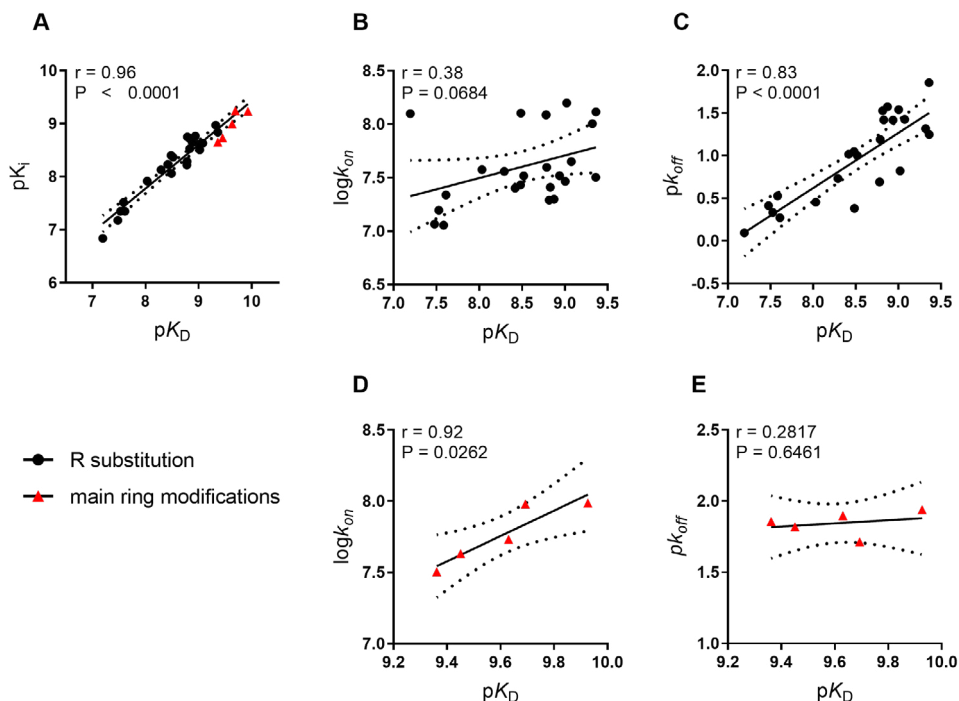


Figure 3: Correlation between affinity determined from typical displacement assays (pK_i) and kinetic affinity determined based on parameters k_{on} and k_{off} obtained from competition association assays (pK_D) (A); affinity (pK_i) and association rate constant (log k_{on}) of compounds sharing the same scaffold and different R substituents (inhibitors **1** - **25**) (B); affinity (pK_i) and dissociation rate constant (pK_{off}) of compounds sharing the same scaffold and different R substituents (inhibitors **1** - **25**) (C); affinity (pK_i) and association rate constant (log k_{on}) of compounds having different scaffolds (inhibitors **25** - **29**) (D); affinity (pK_i) and dissociation rate constant (pK_{off}) of compounds having different scaffolds (inhibitors **25** - **29**) (E). The solid line corresponds to the linear regression of the data and the dotted lines represent the 95% confidence intervals for regression. Inhibitors with modifications at the main ring are blue and inhibitors with R substituents are represented by the black dots. Data used in the plots are detailed in Tables 1-3. Data are expressed as mean from at least three independent experiments performed in duplicate.

Possible correlations to physicochemical properties of the phenyl's *meta* substituents (R) were also examined (Supplementary Figure S2). The acid dissociation constants (pK_a) as well as the distribution-coefficient (logD) at pH 7.4 of the substituents were investigated. No correlation was found between the association

rate constants ($\log k_{on}$) and pK_a ($r=0.247$, $P=0.2798$) or $\log D$ ($r=0.164$, $P=0.4327$). Affinity (pK_D) and dissociation rate constant (pK_{off}) appeared correlated with pK_a ($r=-0.657$, $P=0.0012$ and $r=-0.695$, $P=0.0003$, respectively). As a result, all inhibitors with an easily protonated functional group R (**12-13**, **16-17**, **23-24**), demonstrate a lower affinity and shorter RT compared to the non-protonated functional groups (**11**, **14-15**, **18-19**, **25**) at pH 7.4. These findings are suggestive of a sub-pocket where a positive charge is not easily accommodated. Evidence in 3D-QSAR models was found for electronegative substituents near the *para*-position of the S^6 -benzyl substituent of NBTI to be favorable, supporting our findings^{32, 33}. Likewise, pK_D and pK_{off} were correlated with $\log D$ ($r=0.636$, $P=0.0008$ and $r=0.655$, $P=0.0004$, respectively) providing evidence that R substituents' hydrophobicity plays a role in affinity and RT. This suggests hydrophobic amino acids to be present in the sub-pocket of the binding site of ENT1. Such a trend has already been described in the literature for existing ENT1 inhibitors. A hydrophobic group at the purine 6-position of NBTI has been found to be important for high affinity binding to ENT1³²⁻³⁴. This functionality is also represented by the *bis*-fluorophenyl functional group of draflazine, which contributed to a high binding affinity³⁵. In addition, Tromp *et al.* found a C⁸-cyclopentylamine-substitution in an NBTI-related series of compounds provided the highest affinity³⁶. 3D-QSAR modeling also showed the ENT1 pharmacophore to consist of at least one hydrophobic group^{32, 33}. Finally, our findings are in-line with the recent crystal structure of ENT1, showing that hydrophobic interactions are crucial of the binding of both dilazep and NBTI³⁷.

Conclusions

In this study, a series of spirobenzo-oxazinepiperidinone derivatives designed as ENT1 inhibitors were tested for their affinity and target binding kinetics by performing radioligand binding assays. Structure-kinetic relationships were examined in addition to structure-affinity relationships to define which functional groups are involved in binding to ENT1. It was found that bulkier substituents at the "right-hand" phenyl ring were well tolerated, suggesting a large binding pocket for ENT1. These substituents provided high affinity and a long RT when being hydrophobic or uncharged at physiological pH. Additionally, it was found that the compounds tested associate faster to the transporter when the polarity of the central scaffold is reduced. By and large, this study may contribute to the development of inhibitors with a high affinity and optimal binding kinetics at ENT1, and, more generally, pave the way for similar studies at other transport proteins.

Experimental Section

Chemicals and Reagents.

Bovine serum albumin (BSA) and the bicinchoninic acid (BCA) protein assay kit were purchased from Fisher Scientific (Hampton, New Hampshire, United States). [^3H] NBTI (specific activity 33.1 Ci mmol $^{-1}$) was purchased from PerkinElmer (Groningen, The Netherlands) and NBTI was obtained from Sigma-Aldrich (Steinheim, Germany). Erythrocytes were obtained from Sanquin (Amsterdam, the Netherlands). All other chemicals were purchased from standard commercial sources. All new ENT1 inhibitors were synthesized at Janssen Pharmaceutica (Beerse, Belgium), and checked for identity and purity.

Membrane Preparation.

Erythrocyte membrane preparation was performed as previously described²¹. Membrane protein concentrations were measured using the BCA method³⁸.

Radioligand Binding Assays.

Membranes were thawed and homogenized using an Ultra Turrax homogenizer at 24,000 rpm. Assay buffer (50 mM Tris-HCl pH 7.4, 0.1% (w/v) CHAPS) was used to dilute to the samples to a total reaction volume of 100 μL (except for the wash-out assay where it was 400 μL) containing 1 μg membrane protein and 4 nM [^3H]NBTI. Assay buffer, (radio)ligands and membranes were cooled at 10 $^{\circ}\text{C}$ prior to the experiment. Incubations were performed at 10 $^{\circ}\text{C}$. Nonspecific binding was determined at the presence of 10 μM NBTI. In all cases, DMSO concentrations were kept $\leq 0.25\%$ and total binding did not exceed 10% of the [^3H]NBTI present in the assay in order to prevent ligand depletion. All radioligand binding assays were performed as previously described²¹.

In short, *displacement experiments* were performed using [^3H]NBTI and a competing unlabeled ligand at multiple concentrations. Samples incubation lasted for 1 h was terminated by rapid vacuum filtration over 96-well Whatman GF/C filter plates using a PerkinElmer Filtermate harvester (PerkinElmer, Groningen, Netherlands). Subsequently, filters were washed ten times using ice-cold wash buffer (50 mM Tris-HCl, pH 7.4) and filter-bound radioactivity was determined by liquid scintillation spectrometry using a 2450 Microbeta² scintillation counter (PerkinElmer).

Wash-out experiments were performed by the incubation of inhibitors **18**, **23**, and **25** at their $10 \times \text{IC}_{50}$ with erythrocyte membranes for 1 h while gently shaking. Centrifugation at 13,200 rpm (16,100g) at 4 $^{\circ}\text{C}$ for 5 min separated pellet and supernatant, with the latter containing the unbound ligand being removed. Pellets were resuspended in 1 mL of assay buffer, and samples were incubated for 10 min

at 10 °C. In total four centrifugation-washing cycles were performed. The pellet-membranes were resuspended in a total volume of 400 µL containing [³H]NBTI and were incubated for 1 h. Rapid filtration through GF/C filters using a Brandel harvester (Brandel, Gaithersburg, MD) terminated the experiment. Filters were washed three times using ice-cold wash buffer the samples were counted by scintillation spectrometry using a Tri-carb 2900 TR liquid scintillation counter (Perkin Elmer, Boston, MA).

Competition association experiments were carried out by incubation of [³H]NBTI and a competing ligand at its IC₅₀ concentration. The amount of transporter-bound radioligand was determined at different time points up to 1 h. The samples were obtained and quantified as described under “*displacement experiments*”.

Data Analysis.

Data analyses were performed using GraphPad Prism 7.0 software (GraphPad Software Inc., San Diego, CA, USA). For displacement assays, pIC₅₀ values were obtained by non-linear regression curve fitting to a sigmoidal concentration-response curve using the equation: $Y = \text{Bottom} + (\text{Top} - \text{Bottom}) / (1 + 10^{-(X - \text{LogIC}_{50})})$. pK_i values were converted from pIC₅₀ and the saturation K_D values using the ChengPrusoff equation³⁹:

$$K_i = \text{IC}_{50} / (1 + [\text{radioligand}] / K_D)$$

Association and dissociation rate constants for unlabelled ENT1 inhibitors were determined by nonlinear regression analysis of competition association data as described by Motulsky and Mahan²².

$$\begin{aligned} K_A &= k_1[L] \cdot 10^{-9} + k_2 \\ K_B &= k_3[I] \cdot 10^{-9} + k_4 \\ S &= \sqrt{(K_A - K_B)^2 + 4 \cdot k_1 \cdot k_3 \cdot L \cdot I \cdot 10^{-18}} \\ K_F &= 0.5(K_A + K_B + S) \\ K_S &= 0.5(K_A + K_B - S) \\ Q &= \frac{B_{\max} \cdot k_1 \cdot L \cdot 10^{-9}}{K_F - K_S} \\ Y &= Q \left(\frac{k_4(K_F - K_S)}{K_F \cdot K_S} + \frac{k_4 - K_F}{K_F} e^{(-K_F \cdot X)} - \frac{k_4 - K_S}{K_S} e^{(-K_S \cdot X)} \right) \end{aligned}$$

Where k_1 and k_2 are the k_{on} (M⁻¹min⁻¹) and k_{off} (min⁻¹) of [³H]NBTI, respectively, L is the radioligand concentration (nM), I is the concentration of unlabeled competitor (nM), Y is the specific binding of the radioligand (DPM) and X is the time (min). Fixing these parameters with the help of a control curve, where no unlabeled compound was used, allows the calculation of the following parameters: k_3 (M⁻¹min⁻¹), which is the k_{on} value of the unlabeled ligand; k_4 (min⁻¹), which is the k_{off} value of the unlabeled

ligand and B_{\max} that equals the total binding (DPM). All competition association data were globally fitted. The residence time (RT) was calculated using $RT = 1 / k_{\text{off}}$ ⁴⁰. The kinetic affinity K_D was calculated by association and dissociation rates using the following equation:

$$K_D = k_{\text{off}} / k_{\text{on}}$$

logD and pKa values were calculated using the Chemicalize platform from ChemAxon. All values are shown as mean \pm S.E.M. of at least three independent experiments performed in duplicate. Statistical analysis was performed if indicated, using a one-way ANOVA with Dunnett's post-test (###P < 0.001; ##P < 0.01; #P < 0.05) or an unpaired Student's t test (***P < 0.001; **P < 0.01; *P < 0.05). Observed differences were considered statistically significant if P-values were below 0.05.

References

1. Young, J. D.; Yao, S. Y.; Baldwin, J. M.; Cass, C. E.; Baldwin, S. A. The human concentrative and equilibrative nucleoside transporter families, SLC28 and SLC29. *Mol Aspects Med* **2013**, 34, 529-47.
2. Rehan, S.; Ashok, Y.; Nanekar, R.; Jaakola, V. P. Thermodynamics and kinetics of inhibitor binding to human equilibrative nucleoside transporter subtype-1. *Biochem Pharmacol* **2015**, 98, 681-9.
3. Blackburn, G. M.; Gait, M. J.; Loakes, D.; Williams, D. M. Nucleosides and Nucleotides. In *Nucleic Acids in Chemistry and Biology: Edition 3*, Royal Society of Chemistry: 2006; pp 125-135.
4. Damaraju, V. L.; Damaraju, S.; Young, J. D.; Baldwin, S. A.; Mackey, J.; Sawyer, M. B.; Cass, C. E. Nucleoside anticancer drugs: the role of nucleoside transporters in resistance to cancer chemotherapy. *Oncogene* **2003**, 22, 7524-36.
5. Zhang, J.; Visser, F.; King, K. M.; Baldwin, S. A.; Young, J. D.; Cass, C. E. The role of nucleoside transporters in cancer chemotherapy with nucleoside drugs. *Cancer Metastasis Rev* **2007**, 26, 85-110.
6. Jordheim, L. P.; Durantel, D.; Zoulim, F.; Dumontet, C. Advances in the development of nucleoside and nucleotide analogues for cancer and viral diseases. *Nat Rev Drug Discov* **2013**, 12, 447-64.
7. Quashie, N. B.; Ranford-Cartwright, L. C.; de Koning, H. P. Uptake of purines in Plasmodium falciparum-infected human erythrocytes is mostly mediated by the human equilibrative nucleoside transporter and the human facilitative nucleobase transporter. *Malar J* **2010**, 9, 36.
8. Molina-Arcas, M.; Casado, F. J.; Pastor-Anglada, M. Nucleoside transporter proteins. *Curr Vasc Pharmacol* **2009**, 7, 426-34.

9. Mangravite, L. M.; Xiao, G.; Giacomini, K. M. Localization of human equilibrative nucleoside transporters, hENT1 and hENT2, in renal epithelial cells. *Am J Physiol Renal Physiol* **2003**, 284, F902-10.
10. Baldwin, S. A.; Beal, P. R.; Yao, S. Y.; King, A. E.; Cass, C. E.; Young, J. D. The equilibrative nucleoside transporter family, SLC29. *Pflugers Arch* **2004**, 447, 735-43.
11. Pastor-Anglada, M.; Perez-Torras, S. Emerging Roles of Nucleoside Transporters. *Front Pharmacol* **2018**, 9, 606.
12. Lane, J.; Martin, T. A.; McGuigan, C.; Mason, M. D.; Jiang, W. G. The differential expression of hCNT1 and hENT1 in breast cancer and the possible impact on breast cancer therapy. *J Exp Ther Oncol* **2010**, 8, 203-10.
13. Greenhalf, W.; Ghaneh, P.; Neoptolemos, J. P.; Palmer, D. H.; Cox, T. F.; Lamb, R. F.; Garner, E.; Campbell, F.; Mackey, J. R.; Costello, E.; Moore, M. J.; Valle, J. W.; McDonald, A. C.; Carter, R.; Tebbutt, N. C.; Goldstein, D.; Shannon, J.; Dervenis, C.; Glimelius, B.; Deakin, M.; Charnley, R. M.; Lacaine, F.; Scarfe, A. G.; Middleton, M. R.; Anthoney, A.; Halloran, C. M.; Mayerle, J.; Olah, A.; Jackson, R.; Rawcliffe, C. L.; Scarpa, A.; Bassi, C.; Buchler, M. W. Pancreatic cancer hENT1 expression and survival from gemcitabine in patients from the ESPAC-3 trial. *J Natl Cancer Inst* **2014**, 106, djt347.
14. Pennycooke, M.; Chaudary, N.; Shuralyova, I.; Zhang, Y.; Coe, I. R. Differential expression of human nucleoside transporters in normal and tumor tissue. *Biochem Biophys Res Commun* **2001**, 280, 951-9.
15. Andersen, K.; Dellborg, M.; Swedberg, K. Nucleoside transport inhibition by draflazine in unstable coronary disease. *Eur J Clin Pharmacol* **1996**, 51, 7-13.
16. Deguchi, H.; Takeya, H.; Wada, H.; Gabazza, E. C.; Hayashi, N.; Urano, H.; Suzuki, K. Dilazep, an antiplatelet agent, inhibits tissue factor expression in endothelial cells and monocytes. *Blood* **1997**, 90, 2345-56.
17. Khalil, A.; Belal, F.; Al-Badr, A. A. Dipyridamole: comprehensive profile. *Profiles Drug Subst Excip Relat Methodol* **2005**, 31, 215-80.
18. Swinney, D. C. The role of binding kinetics in therapeutically useful drug action. *Curr Opin Drug Discov Devel* **2009**, 12, 31-9.
19. Guo, D.; Hillger, J. M.; IJzerman, A. P.; Heitman, L. H. Drug-target residence time--a case for G protein-coupled receptors. *Med Res Rev* **2014**, 34, 856-92.
20. Copeland, R. A. The drug-target residence time model: a 10-year retrospective. *Nat Rev Drug Discov* **2016**, 15, 87-95.
21. Vlachodimou, A.; Konstantinopoulou, K.; IJzerman, A. P.; Heitman, L. H. Affinity, binding kinetics and functional characterization of draflazine analogues for human equilibrative nucleoside transporter 1 (SLC29A1). *Biochemical Pharmacology* **2020**, 172, 113747.
22. Motulsky, H. J.; Mahan, L. C. The kinetics of competitive radioligand binding predicted by the law of mass action. *Mol Pharmacol* **1984**, 25, 1-9.
23. Doornbos, M. L. J.; Cid, J. M.; Haubrich, J.; Nunes, A.; van de Sande, J. W.;

- Vermond, S. C.; Mulder-Krieger, T.; Trabanco, A. A.; Ahnaou, A.; Drinkenburg, W. H.; Lavreysen, H.; Heitman, L. H.; IJzerman, A. P.; Tresadern, G. Discovery and Kinetic Profiling of 7-Aryl-1,2,4-triazolo[4,3-a]pyridines: Positive Allosteric Modulators of the Metabotropic Glutamate Receptor 2. *Journal of Medicinal Chemistry* **2017**, 60, 6704-6720.
24. de Witte, W. E. A.; Vauquelin, G.; van der Graaf, P. H.; de Lange, E. C. M. The influence of drug distribution and drug-target binding on target occupancy: The rate-limiting step approximation. *Eur J Pharm Sci* **2017**, 109s, S83-s89.
25. Vauquelin, G.; Charlton, S. J. Long-lasting target binding and rebinding as mechanisms to prolong in vivo drug action. *British Journal of Pharmacology* **2010**, 161, 488-508.
26. Xia, L.; Burger, W. A. C.; van Veldhoven, J. P. D.; Kuiper, B. J.; van Duijl, T. T.; Lenselink, E. B.; Paasman, E.; Heitman, L. H.; IJzerman, A. P. Structure-Affinity Relationships and Structure-Kinetics Relationships of Pyrido[2,1-f]purine-2,4-dione Derivatives as Human Adenosine A3 Receptor Antagonists. *Journal of Medicinal Chemistry* **2017**, 60, 7555-7568.
27. de Witte, W. E. A.; Danhof, M.; van der Graaf, P. H.; de Lange, E. C. M. In vivo Target Residence Time and Kinetic Selectivity: The Association Rate Constant as Determinant. *Trends Pharmacol Sci* **2016**, 37, 831-842.
28. Schoop, A.; Dey, F. On-rate based optimization of structure-kinetic relationship-surfing the kinetic map. *Drug Discov Today Technol* **2015**, 17, 9-15.
29. Vauquelin, G. Effects of target binding kinetics on in vivo drug efficacy: koff, kon and rebinding. *Br J Pharmacol* **2016**, 173, 2319-34.
30. Tummino, P. J.; Copeland, R. A. Residence Time of Receptor-Ligand Complexes and Its Effect on Biological Function. *Biochemistry* **2008**, 47, 5481-5492.
31. Tonge, P. J. Drug-Target Kinetics in Drug Discovery. *ACS Chem Neurosci* **2018**, 9, 29-39.
32. Gupte, A.; Buolamwini, J. K. CoMFA and CoMSIA 3D-QSAR studies on S6-(4-nitrobenzyl)mercaptapurine riboside (NBMPR) analogs as inhibitors of human equilibrative nucleoside transporter 1 (hENT1). *Bioorganic & Medicinal Chemistry Letters* **2009**, 19, 314-318.
33. Zhu, Z.; Buolamwini, J. K. Constrained NBMPR Analogue Synthesis, Pharmacophore Mapping and 3D-QSAR Modeling of Equilibrative nucleoside Transporter 1 (ENT1) Inhibitory Activity. *Bioorganic & medicinal chemistry* **2008**, 16, 3848-3865.
34. Gupte, A.; Buolamwini, J. K. Novel halogenated nitrobenzylthioinosine analogs as es nucleoside transporter inhibitors. *Bioorg Med Chem Lett* **2004**, 14, 2257-60.
35. Hammond, J. R. Interaction of a series of draflazine analogues with equilibrative nucleoside transporters: species differences and transporter subtype selectivity. *Naunyn Schmiedebergs Arch Pharmacol* **2000**, 361, 373-82.
36. Tromp, R. A.; Spanjersberg, R. F.; von Frijtag Drabbe Künzel, J. K.; IJzerman, A. P. Inhibition of Nucleoside Transport Proteins by C8-Alkylamine-Substituted

- Purines. *Journal of Medicinal Chemistry* **2005**, 48, 321-329.
37. Wright, N. J.; Lee, S.-Y. Structures of human ENT1 in complex with adenosine reuptake inhibitors. *Nature Structural & Molecular Biology* **2019**, 26, 599-606.
38. Smith, P. K.; Krohn, R. I.; Hermanson, G. T.; Mallia, A. K.; Gartner, F. H.; Provenzano, M. D.; Fujimoto, E. K.; Goeke, N. M.; Olson, B. J.; Klenk, D. C. Measurement of protein using bicinchoninic acid. *Anal Biochem* **1985**, 150, 76-85.
39. Cheng, Y.; Prusoff, W. H. Relationship between the inhibition constant (KI) and the concentration of inhibitor which causes 50 per cent inhibition (I50) of an enzymatic reaction. *Biochemical Pharmacology* **1973**, 22, 3099-3108.
40. Copeland, R. A. Evaluation of enzyme inhibitors in drug discovery. A guide for medicinal chemists and pharmacologists. *Methods Biochem Anal* **2005**, 46, 1-265.

Supplementary material

The physicochemical parameters of the R substituents were calculated using the Chemicalize platform from ChemAxon. The pK_a and logD values are displayed in the Table S1 and correspond to the phenyl ring together with the R substituent (marked in blue in Supplementary Figure S1). The pK_a values were determined for the amine or oxygen on the phenyl *para*-position or the rest of amine and oxygens of the R substituents. We continued to the latter case, only when no ionization occurred in the first instance. The logD values were calculated at pH 7.4.

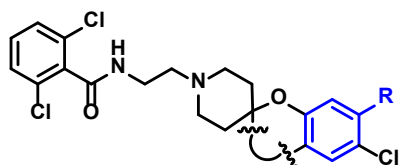


Figure S1: Structure of the ENT1 inhibitors and the subpart of the structure used for the pK_a and logD calculations (marked in blue).

Table S1: pK_a and logD (at pH 7.4) values calculated for the phenyl ring including the R substituent of compounds **1 – 25** (see Figure S1).

| compd | pK_a (of N/O) | logD (at pH 7.4) |
|-------|----------------------------------------|------------------|
| 1 | 4.64 ^a | 1.14 |
| 2 | 4.68 ^a | 1.45 |
| 3 | 5.02 ^a | 2.08 |
| 4 | 14.38 ^a | 1.21 |
| 5 | 5.36 ^a | 1.86 |
| 6 | 5.04 ^a | 2.80 |
| 7 | 5.19 ^a | 3.11 |
| 8 | 3.93 ^a , 10.22 ^b | -1.54 |
| 9 | 5.00 ^a | 0.53 |
| 10 | 4.86 ^a | 2.2 |
| 11 | 1.43 ^a | 1.86 |
| 12 | 8.89 ^b , -0.32 ^a | 0.05 |
| 13 | 7.95 ^b , -0.88 ^a | 1.27 |
| 14 | 3.41 ^a | 2.83 |
| 15 | 4.86 ^a | 1.41 |
| 16 | 9.98 ^b , 3.63 ^a | -1.41 |
| 17 | 8.90 ^b , 3.31 ^a | -0.04 |
| 18 | 4.88 ^a , -1.36 ^b | 0.70 |
| 19 | 4.7 ^a | 2.37 |
| 20 | N.D. | N.D. |
| 21 | No ionizable atoms found | 2.59 |
| 22 | No ionizable atoms found | 3.17 |
| 23 | 9.82 ^b | -0.90 |
| 24 | 8.6 ^b | 0.62 |
| 25 | -1.28 ^b | 1.07 |

^a Ionization of 4-N or 4-O. ^b Ionization of second substituted N or O. N.D. not determined

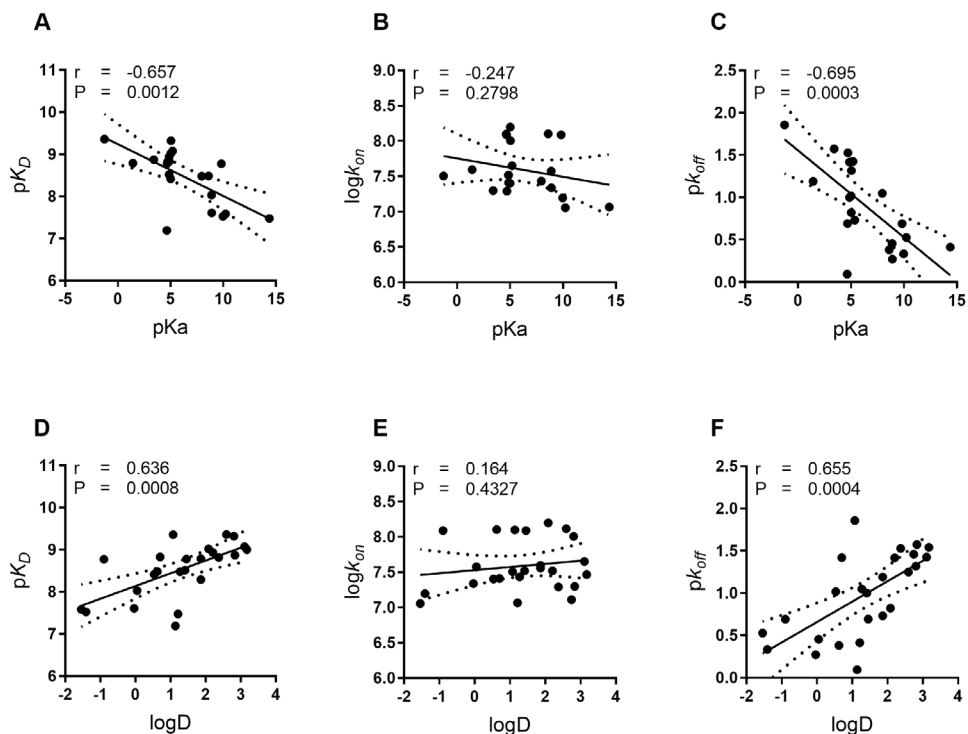


Figure S2: Correlation between affinity (pK_i), association rate constant ($\log k_{on}$) and dissociation rate constant (pK_{off}) of inhibitors 1 – 25 versus acid dissociation constant (pK_a) and distribution-coefficient ($\log D$) of the substituent R.

(A); association rate constant ($\log k_{on}$) and acid dissociation constant (pK_a) of substituent R (B); dissociation rate constant (pK_{off}) and acid dissociation constant (pK_a) of substituent R (C). Correlation between affinity (pK_i) and distribution-coefficient ($\log D$) of substituent R (D); association rate constant ($\log k_{on}$) and distribution-coefficient ($\log D$) of substituent R (E); dissociation rate constant (pK_{off}) and distribution-coefficient ($\log D$) of substituent R (F). For all graphs, affinity (pK_i), association ($\log k_{on}$) and dissociation (pK_{off}) rate constants are the values obtained for the binding of the whole molecule to the transporter. On the other hand, the acid dissociation constant (pK_a) and the distribution-coefficient ($\log D$) were calculated only for the R substituent. The solid line corresponds to the linear regression of the data, the dotted lines represent the 95% confidence intervals for regression. Inhibitors with modifications at the main ring are blue and inhibitors with R substituents are represented by the black dots. Data used in the plots are detailed in Tables 1-5. Experimental data are expressed as mean from at least three independent experiments performed in duplicate.

